Geophysical Research Letters

RESEARCH LETTER
10.1029/2025GL121372

Mesoscale Soil Moisture Heterogeneity Can Locally Amplify Humid Heat

G. Chagnaud[1], C. M. Taylor[1,2], L. S. Jackson[3], A. Barber[3,4], H. Burns[3,4], J. H. Marsham[3,5], and C. E. Birch[3]

[1]UK Centre for Ecology and Hydrology, Wallingford, UK, [2]National Centre for Earth Observation, Wallingford, UK, [3]School of Earth and Environment, University of Leeds, Leeds, UK, [4]Centre for Environmental Modelling and Computation, University of Leeds, Leeds, UK, [5]Met Office, Exeter, UK

Key Points:

- Humid heat associated with soil moisture heterogeneity is locally amplified by 1–4°C as compared to uniform wet soil
- Subsidence due to soil moisture-induced mesoscale circulations more efficiently concentrates warm, humid air in a shallower boundary layer
- Background wind and wet-dry contrast magnitude control the relationship between soil moisture length-scale and humid heat amplification

Supporting Information:

Supporting Information may be found in the online version of this article.

Correspondence to:

G. Chagnaud,
guicha@ceh.ac.uk

Citation:

Chagnaud, G., Taylor, C. M., Jackson, L. S., Barber, A., Burns, H., Marsham, J. H., & Birch, C. E. (2026). Mesoscale soil moisture heterogeneity can locally amplify humid heat. *Geophysical Research Letters*, *53*, e2025GL121372. https://doi.org/10.1029/2025GL121372

Received 9 JAN 2026
Accepted 24 APR 2026

Author Contributions:

Conceptualization: G. Chagnaud, C. M. Taylor, J. H. Marsham, C. E. Birch
Data curation: G. Chagnaud
Formal analysis: G. Chagnaud
Funding acquisition: C. M. Taylor, C. E. Birch
Investigation: G. Chagnaud, C. M. Taylor, L. S. Jackson, J. H. Marsham, C. E. Birch
Methodology: G. Chagnaud, C. M. Taylor, J. H. Marsham, C. E. Birch
Resources: A. Barber, H. Burns
Writing – original draft: G. Chagnaud
Writing – review & editing: G. Chagnaud, C. M. Taylor, L. S. Jackson, A. Barber, H. Burns, J. H. Marsham, C. E. Birch

Abstract Soil moisture is a key ingredient of humid heat through supplying moisture and modifying boundary layer properties. Soil moisture heterogeneity due to for example, antecedent rainfall, can strongly influence weather patterns; yet, its effect on humid heat is poorly understood. Idealized numerical simulations are performed with a cloud-resolving ($\Delta x = 500$ m), coupled land-atmosphere model wherein wet patches on length-scales $\lambda \in 25$–150 km are prescribed. Compared to experiments with uniform soil moisture, humid heat is locally amplified by 1–4°C, with maximum amplification for the critical soil moisture length-scale $\lambda_c = 50$ km. Subsidence associated with a soil moisture-induced mesoscale circulation concentrates warm, humid air in a shallower boundary layer. The background wind and the magnitude of the wet-dry contrast control the relationship between λ_c and the humid heat amplification. Based on observed soil moisture patterns, these results will help to predict extreme humid heat on city and county scales across the Tropics.

Plain Language Summary Humidity exacerbates human heat stress by limiting the body's cooling through reduced sweat evaporation. Humid heat extremes can occur when additional moisture is supplied in a warm environment, for instance from wetter soils following rainfall. The spatial variability of soil moisture is known to influence weather patterns, but its effects on humid heat are largely unexplored. To investigate how soil moisture heterogeneity influences humid heat, a series of simulations are performed with a high-resolution model of the coupled land-atmosphere system: circular wet patches of length 25–150 km across are imposed in the center of an otherwise dry domain. Compared to a simulation with uniform soil moisture, humid heat is locally larger by 1–4°C with soil moisture heterogeneity. Atmospheric circulations generated by soil moisture contrasts reduce the vertical mixing of air, leading to higher humid heat near the surface than would occur without soil moisture heterogeneity. Our results are robust across different metrics of humid heat and across various environments. They improve mechanistic understanding of humid heat, which will help to better predict hazardous humid heat hours to days in advance across vast swathes of the Tropics.

1. Introduction

The habitats of many terrestrial species are within a few meters above the ground; their living conditions therefore depend largely on weather conditions near the surface, which involve land-atmosphere interactions on a wide range of time and spatial scales (Santanello et al., 2018). Heatwaves, prolonged periods of high heat stress, are among the most detrimental weather phenomena to ecosystems and societies. The increase in the intensity, frequency, and duration of heatwaves as a result of global warming has already caused numerous excess deaths around the world and will continue to do so, even with moderate greenhouse gases emissions (Gasparrini et al., 2017; Matthews, Raymond, et al., 2025; Mitchell et al., 2016; Vicedo-Cabrera et al., 2021).

Humidity is known to exacerbate human heat stress by limiting sweat evaporation. Humid heat can be quantified by various metrics, including wet-bulb temperature (Twb) and Heat Index (HI), and there is no consensus in the literature on which is more relevant to human health. Sherwood and Huber (2010) suggest that an upper survivability limit for fit people is Twb = 35°C (see also Buzan & Huber, 2020). Other studies show that adverse health effects can occur in vulnerable groups after ~6 hr of exposure to Twb ≥ 24–25°C (Vanos et al., 2023; Vecellio et al., 2022), considerably increasing the prevalence of high Twb values as a global heat risk (Vecellio et al., 2023). The all-year 95th percentile of daily mean Twb (Twbd-95) is 24°C on average in the Tropics and above 25°C in many coastal and inland low-lying areas (Figure S1a in Supporting Information S1). In addition,

there is strong seasonality in the timing of Twbd-95 (Figure S1b in Supporting Information S1), as dictated, for example, by the onset or cessation of rainy seasons (Ivanovich et al., 2024; Jackson et al., 2025).

Recent studies have demonstrated that the highest Twb values are tied to large-scale atmospheric dynamics through stability and entrainment (Duan et al., 2024; Li & Tamarin-Brodsky, 2026; Y. Zhang et al., 2021), but they also acknowledge that local processes can lead to extreme humid heat. Wet soils, driven, for instance, by antecedent rainfall or irrigation, support higher humid heat in southern Asia (Mishra et al., 2020; Monteiro & Caballero, 2019), the US (L. Chen et al., 2025; Gurung & Chen, 2024; Krakauer et al., 2020), China (S. Kang & Eltahir, 2018; Yan et al., 2025; Zou et al., 2024), and across sub-Saharan Africa (Chagnaud et al., 2025). Soil moisture (SM) can exert a strong control on near-surface humid heat through surface latent heat flux (LHF) being enhanced at the expense of surface sensible heat flux (SHF), which limits the growth of the boundary layer (BL) and concentrates more humid air in a shallower BL (Chagnaud et al., 2025; Jackson et al., 2025; Kong & Huber, 2023; Mishra et al., 2020). This "volume reduction" mechanism is especially efficient in regions/seasons where SM exerts a first-order control on the partitioning of available (radiative) energy, R_{net}, into surface heat fluxes. This typically occurs when (a) insolation is abundant (i.e., cloud cover is minimal), and (b) soil moisture sits between the wilting point (θ_W), below which soils are largely dry, and the critical point (θ_C), above which soils are wet; the SM–evaporative fraction (EF = LHF/R_{net}) relationship then belongs to the water-limited regime and is said to be "transitional" (Dirmeyer, 2011; Seneviratne et al., 2010). The SM–EF regime is transitional in large swathes of sub-Saharan Africa, India, and Central America more than 50% of the time during the humid heat season (Figure S1c in Supporting Information S1).

On daily timescales, soil moisture can exhibit spatial variability over distances ranging from a few hundred meters to several tens of kilometers. Spatial heterogeneity is a ubiquitous property of soil moisture in the Tropics (Figure S1d in Supporting Information S1). In the transitional SM–EF regime, spatial SHF contrasts resulting from soil moisture heterogeneity can trigger mesoscale circulations, in turn influencing the land surface–BL coupling. Having been extensively studied with a diversity of observational (Barton et al., 2020; Bhumralkar, 1973; Dixon et al., 2013; Mahrt et al., 1994; Taylor et al., 2007), analytical (Dalu & Pielke, 1993; Green & Dalu, 1980; Segal & Arritt, 1992) and numerical approaches (Chen & Avissar, 1994; Han et al., 2019; Kang & Davis, 2008; Ookouchi et al., 1984; Patton et al., 2005; Pielke et al., 1991; Van Heerwaarden et al., 2014; Wang et al., 1998; L. Zhang et al., 2023), mesoscale circulations are enhanced for a range of spatial heterogeneity length-scales (λ). Furthermore, the large-scale wind, the amplitude of surface heterogeneity, and the thermodynamical structure of the atmosphere modulate the way mesoscale circulations form, grow, and decay.

The impacts of mesoscale circulations on land surface–BL coupling have been widely studied from the perspective of convection (see above references); yet, their effects on humid heat remain largely unexplored. Averaging across more than 200 heatwaves from a pan-African, convection-permitting model simulation, Chagnaud et al. (2025) found a mesoscale circulation and reduced BL height (z_i) in cases associated with positive soil moisture anomalies at $\lambda \approx 50$ km. In these events, Twb was amplified by 0.5–0.6°C compared to events associated with larger-scale soil moisture anomalies, where a mesoscale circulation was absent. This study suggests a pathway whereby soil moisture heterogeneity influences Twb extremes, calling for further investigation of the relationship between humid heat and soil moisture length-scale.

We examine how soil moisture heterogeneity influences near-surface humid heat by performing idealized simulations with a convection-resolving ($\Delta x = 500$ m), coupled land-atmosphere model. The objectives are to determine (a) whether a critical soil moisture length-scale λ_c exists for which the effect on humid heat is maximized and, if so, (b) what are the mechanisms involved, and (c) how does λ_c vary with environmental conditions and humid heat metrics. In addition to improving our understanding of the role of fine-scale land-atmosphere interactions in humid heat, providing answers to these questions would improve our capacity to use satellite observations of soil moisture—available even in regions of sparse weather station networks—in combination with numerical weather models to predict humid heat extremes.

2. Methods

2.1. Idealized Configuration of the Met Office Unified Model

A series of simulations were run using an idealized configuration of the Met Office Unified Model (UM) coupled to the Joint UK Land Environment Simulator (JULES). The UM science configuration is based on version 3 of the

Regional Atmosphere and Land configuration (Bush et al., 2024). The non-hydrostatic, fully compressible equations of motion are discretized on a 400 km × 400 km cartesian grid with 500 m horizontal grid spacing and solved with the ENDGame dynamical core (Wood et al., 2014), the time step of integration being 20 s. In the vertical, the model uses a Charney–Phillips grid (Charney & Phillips, 1953) with 90 levels, of which 67 are below 18 km, and a fixed model lid 40 km above the surface. Key parameterizations include radiation (Edwards & Slingo, 1996), microphysics (Field et al., 2023), and turbulence (Boutle et al., 2014). The surface–atmosphere exchanges of momentum, mass, and energy, together with the surface and sub-surface flows of water and heat are treated in JULES (Best et al., 2011). Similar UM configurations have been used to study the atmospheric impacts of irrigation over India (Fletcher et al., 2022), the effect of soil moisture variability on Sahelian storms (Maybee et al., 2025), and to test convection parameterization schemes (Lavender et al., 2024). The UM has also been run in a non-idealized configuration for climate and climate change studies at convection-permitting scales over Africa (Birch et al., 2022; Kendon et al., 2019; Stratton et al., 2018).

2.2. Experimental Setup and Simulations

To avoid contamination of soil moisture-induced circulations by flows due to topographic or vegetation heterogeneity, flat terrain and bare soil are used throughout the model domain. The hydraulic properties of bare soil are set to that of sand: the volumetric soil moisture content at wilting point and critical point are $\theta_W = 0.045$ $m^3\ m^{-3}$ and $\theta_C = 0.128\ m^3\ m^{-3}$, respectively (Dharssi et al., 2009). The roughness lengths for momentum and scalars are set to $z_{0,m} = 10$ cm and $z_{0,h} = 2$ cm, corresponding to what would be found on tropical grassland of height $h = 1$ m with $z_{0,m}$ parameterized as $z_{0,m} = h/10$ and $z_{0,h}/z_{0,m} = 0.2$ (Best et al., 2011; Stratton et al., 2018). We use radiosonde observations of temperature and humidity from the African Monsoon Multidisciplinary Analysis field campaign (Parker et al., 2008), with cyclic lateral boundary conditions mimicking an infinite domain and without large-scale advection of either quantity, as in Lavender et al. (2024). The background wind speed, U, is set to 4 m s^{-1}, consistent with the average large-scale wind speed found at lower atmospheric levels during heatwaves in Chagnaud et al. (2025). U flows from West to East and has a constant vertical profile. The simulations are initialized at midnight and run freely for 24 hr with the diurnal cycle of insolation of Niamey on 10 July, peaking at 950 W m^{-2} at 1200 local time (LT). This configuration forms the reference setup.

We perform two control simulations with uniformly dry and uniformly wet soils, respectively labeled UDRY and UWET. In UDRY, soil moisture is initialized at $0.3 \times \theta_C$ in the four soil layers. In UWET, soil moisture is initialized at θ_C everywhere. To reproduce soil moisture heterogeneity typically induced by rainfall or irrigation, we perform simulations where a soil moisture perturbation is prescribed as a circular wet patch positioned in the center of the domain (see example in Figure 1): soil moisture is initialized at θ_C in the patch and $0.3{\times}\theta_C$ elsewhere, in all soil layers. This soil moisture contrast (δ) allows a direct comparison between perturbed and control simulations. The diameter of the patch, λ, varies from 25 to 150 km; each perturbed simulation is accordingly labeled Pλ (Table 1). Restricting patch sizes to $\lambda \leq 150$ km ensures that soil moisture-induced circulations remain within the limits of the domain. Model diagnostics are output as hourly means to minimize the impact of turbulence. Additional sets of UWET–Pλ simulations are performed to evaluate the sensitivity of the λ–humid heat relationship to U, δ, the vertical profiles of potential temperature (γ_θ) and humidity (γ_q) (Table 1 and Text S2 in Supporting Information S1).

Examining BL properties and surface energy budget terms in control simulations shows that, in the range of soil moisture values utilized here, the BL is very sensitive to the land surface (Figure S2 and Text S3 in Supporting Information S1), as summarized by 1200 LT SHF and 1500 LT z_i values that are more than double in UDRY compared to UWET (Table 1). Since cloud cover remains low (Figure S3 in Supporting Information S1) and no significant rainfall occurs (not shown), this land surface–BL coupling regime remains similar throughout the simulations.

2.3. Calculation of Humid Heat Metrics

Wet-bulb temperature is calculated with the Davies-Jones formula (Davies-Jones, 2008) using hourly near-surface dry-bulb temperature (T) and specific humidity (q), and hourly surface pressure. The Heat Index (HI) is calculated following Rothfusz's polynomial approximation of a human thermoregulation model (Steadman, 1979), with a correction applied following Romps and Lu (2022). We conduct our analysis using Twb and compare the results to HI.

Table 1

Experiment Names and Main Characteristics for the Reference Setup (Ref) and the Sensitivity Experiments (Sensitivity): λ Is the Wet Patch Diameter; SM Is the Volumetric Soil Moisture Content in All Soil Layers (in % of θ_C, for Perturbed Runs the Values Are Displayed as Outside–Inside Patch); γ_θ and γ_q Are Respectively the Vertical Gradients of Potential Temperature and Specific Humidity Used as Boundary Conditions (Both Averaged Between the Surface and 10 km); U Is the Background Wind Speed; SHF(1200) and z_i(1500) Are the Domain-Averaged Sensible Heat Flux at 1200 LT and Boundary Layer Height at 1500 LT, Respectively

	Name	λ [km]	SM [%θ_C]	γ_θ [°C km^{-1}]	γ_q [g kg^{-1} km^{-1}]	U [m s^{-1}]	SHF(1200) [W m^{-2}]	z_i(1500) [m]
Ref	UDRY	–	30	4.3	−5.1	4	460	3470
	UWET	–	100	4.3	−5.1	4	163	1678
	Pλ	25, 30, 35, 50, 75, 100, 125, 150	30–100	4.3	−5.1	4	–	–
Sensitivity	$U-$	15, 25, 35, 50, 100	30–100	4.3	−5.1	2	160	1657
	$U+$	25, 50, 100, 150	30–100	4.3	−5.1	8	170	1696
	$\delta-$	25, 50, 100	65–100	4.3	−5.1	4	163	1678
	$\delta+$	25, 50, 100	30–170	4.3	−5.1	4	77	1220
	$\gamma_\theta-$	25, 50, 100	30–100	3.5	−5.1	4	153	1945
	$\gamma_\theta+$	25, 50, 100	30–100	5.1	−5.1	4	180	1387
	γ_q-	25, 50, 100	30–100	4.3	−3.8	4	165	1500
	γ_q+	25, 50, 100	30–100	4.3	−6.4	4	139	1828

Note. SHF(1200) and z_i(1500) values for the Sensitivity setups are from UWET simulations.

3. Results and Discussion

3.1. Near-Surface Atmospheric State in Simulations With Uniform and Heterogeneous Soil Moisture

In the simulation with the 50 km patch (P50), cooler and moister air is found above the wet patch compared to the surroundings (Figures 1a and 1b). The net effect on Twb and HI is an amplification of 2°C and 1°C, respectively, over the wet patch compared to the domain average (Figure 1c and Figure S4a in Supporting Information S1). It is noteworthy that Twb is 2–4°C warmer in UWET compared to UDRY, showing how humid heat is enhanced over wet soil (Figure 1c, inset). The 0800–1900 LT average z_i is 580 m over the wet patch, whereas the domain average is 1,530 m; for reference, the daytime average z_i is 1,555 m in UDRY and 800 m in UWET (Figure 1d, inset). The 10-m wind is slower upwind of the wet patch and faster downwind, compared to uniform soil moisture experiments (Figure 1c).

The four variables also display noticeable sub-daily variability. The wet patch mean Twb has a first peak at 0800 LT and a second, higher peak at 1900 LT (Figure 1c, inset), a bi-modal diurnal cycle typical of semi-arid regions (Birch et al., 2022). Twb values closely follow the diurnal evolution of q (Figure 1b, inset), and the mid-afternoon dip in Twb and q corresponds to the peak in T and z_i. The highest Twb value found at 1900 LT over the wet patch is associated with values of T that are slightly larger than found over uniformly wet soil, alongside larger q and smaller z_i. This analysis highlights the interplay between T, q, and z_i in modulating the space-time structure of Twb. Importantly, Twb and HI are larger over locally wetter soils than found with uniform soil moisture, in association with warmer and more humid air mixed in a shallower BL. Next, we investigate how this local humid heat amplification varies with the length-scale of soil moisture heterogeneity (λ).

3.2. Local Humid Heat Amplification by Mesoscale Soil Moisture Heterogeneity

The diurnal cycle of 3-hourly Twb values peaks at 1900 LT for all wet soil experiments (Figure 2a). In addition, wet patch averages in Pλ are larger than the domain average in UWET when $\lambda \leq 50$ km. Similar pattern is found for HI with a peak at 1800 LT and $\lambda \leq 75$ km (Figure S4b in Supporting Information S1). Hence, peak humid heat values over smaller-scale soil moisture heterogeneity are amplified compared to those over larger-scale wet features.

There is substantial within-patch spatial variability in peak humid heat: visual inspection of Twb fields at 1900 LT reveals that the highest Twb values systematically occur over the downwind half of the patch, that is, between the center of the domain (x_0) and the eastern edge of the patch (Figure S5 in Supporting Information S1). We therefore plot, for each experiment, the 3-hourly Twb averaged over circular areas with radius $r \in$ [5–150 km]

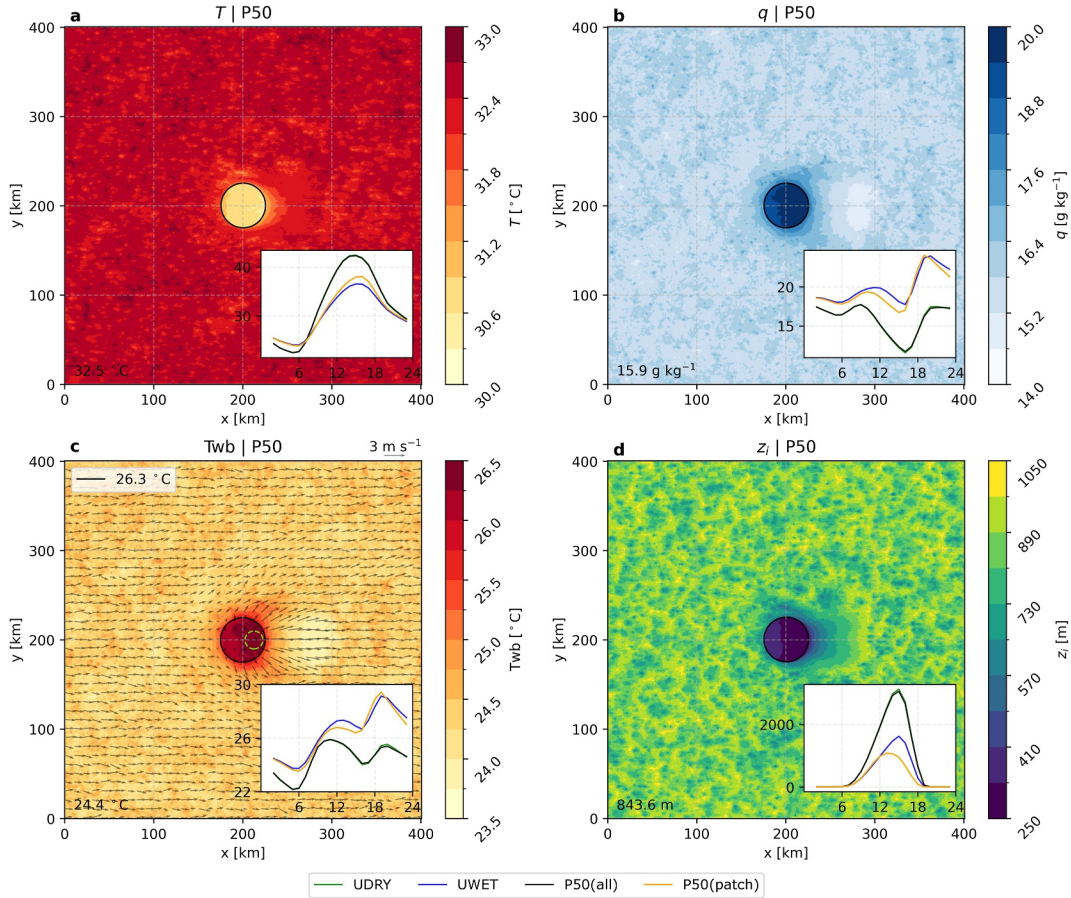

Figure 1. Daily mean (a) T, (b) q, (c) Twb, and (d) z_i in P50. In panel (c) the daily mean 10-m wind is shown with arrows. Insets show spatially averaged evolution of 3-hourly values: green, blue and black lines are domain averages for UDRY, UWET, and P50, respectively; orange line is wet patch average in P50 (see legend). The dashed green circle in panel (c), with radius r =10 km, indicates an area used in Section 3.2.

centered on $x = x_0 + \lambda/4$, denoted $\langle Twb_{max} \rangle_r$ (see an example in Figure 1c for $r = 10$ km). In UDRY and UWET, $\langle Twb_{max} \rangle_r$ is constant with r, reflecting spatial homogeneity (Figure 2b). In perturbed experiments, $\langle Twb_{max} \rangle_r$ has a much stronger dependence on r. Notably, $\langle Twb_{max} \rangle_r$ in perturbed experiments is 0.2–1.2°C larger than in UWET for $r \leq 10$ km, for all λ. This small-scale Twb amplification is largest for $\lambda = 50$ km and reduces for smaller and larger wet patches. A similar behavior is found for the Heat Index, with $\langle HI_{max} \rangle_r$ up to 4°C larger in perturbed than in control experiments for $r < 20$ km and $\lambda \leq 100$ km (Figures S6 and S7 in Supporting Information S1). However, locally higher HI values can be found at other times of day and in different locations (not shown), likely involving other SM-related mechanisms due to the weaker control of humidity on HI compared to Twb (Sherwood, 2018).

This analysis shows that in the experimental setup utilized here, a critical soil moisture length-scale λ_c exists for which humid heat is maximized on length-scales up to 10–20 km across (300–1300 km^2). This area of locally larger Twb/HI values is observed consistently in all perturbed experiments, implying a deterministic cause, in contrast to turbulence-induced pockets of slightly higher humid heat values randomly found in control runs. In the next section, we investigate the land surface–BL coupling with a view to shedding light on the causal chain involved in this local humid heat amplification.

3.3. Soil Moisture-Induced Mesoscale Circulation Control on Boundary Layer Dynamics

In all perturbed experiments, the BL over the area of maximum Twb is shallower than found in their uniform soil moisture counterparts (Figure 3a). This suppressed BL development is especially prominent from noon through to

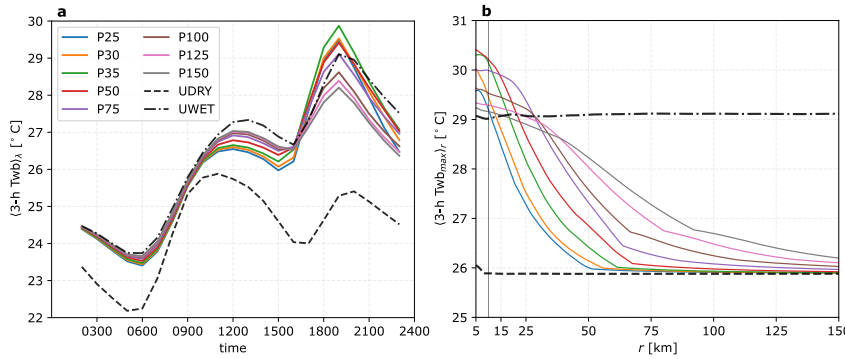

Figure 2. (a) Diurnal cycle of 3-hourly Twb in perturbed experiments (colored lines, see legend), UDRY (dashed line), and UWET (dotted-dashed line). In Pλ, wet patch averages are considered whereas in UDRY and UWET the domain-average Twb is plotted. (b) 1900 LT 3-hourly Twb values averaged over circular areas centered at $x_0 = 200 + \lambda/4$ km and of radius r (in km, horizontal axis) for all perturbed experiments and UWET (see legend in panel (a)).

the evening BL collapse. Figure 3b, which shows for each perturbed experiment, $\langle \mathrm{Twb}_{\max} \rangle_{r=10\ \mathrm{km}}$ as a function of the 1500–1900 LT average z_i, establishes a significant relationship (at the 1% level) between afternoon z_i and evening (peak) Twb (this result is robust to the choice of afternoon window). The inset in Figure 3b shows the strength of the statistical link between Twb sampled at each daytime hour and z_i averaged over the 4 preceding hours: the z_i–Twb relationship is maximized in the late afternoon-evening. This link also holds between afternoon z_i and evening HI, with a linear relationship significant at the 5% level (Figure S8 in Supporting Information S1).

Investigating BL dynamics in response to soil moisture heterogeneity provides process-based insight into the z_i–Twb relationship. Surface turbulent fluxes peak at 1200 LT (Figures S2b and S2d in Supporting Information S1), but the circulation is more intense a few hours later, when the balance between the near-surface pressure gradient that grows in response to the thermal contrast, on the one hand, and the dilution of the thermal contrast through horizontal advection and mixing, on the other hand, is optimal (e.g., Segal & Arritt, 1992). Given the clear relationship between afternoon z_i and evening humid heat amplification (Figure 3b), we examine the BL dynamics during the afternoon.

A well-organized overturning circulation develops in perturbed experiments, as shown with the vertical cross section of potential wet-bulb temperature (θ_{wb}) and wind anomalies at 1500 LT in P50 (Figure 3c). The mesoscale horizontal flow in the longitudinal direction reaches 4–5 m s^{-1} in the lowest atmospheric layers, on both sides of the wet patch; this flow opposes and deflects the background wind on the upwind edge of the patch (Figure 1c), where narrow updrafts develop due to mass conservation. More diffuse downdrafts are located above the wet patch and further downstream. At this time of day, the BL θ_{wb} is 2–3°C cooler in P50 than in UWET except above the wet patch, where this anomaly reduces to ≈ -1°C (Figures 3c and 3d) before turning positive from 1700 LT onward (Figure 2a). In P50, z_i is similar to UDRY over dry areas and, most importantly, lower than in UWET over the wet patch. The subsiding branch of the mesoscale circulation therefore suppresses BL growth above wet soil, as seen in Figure 1d and consistent with previous studies (Heerwaarden & Arellano, 2008; Sühring et al., 2014). Over the wet patch, cloud cover change is limited to ±10% (Figure S9a in Supporting Information S1), resulting in a R_{net} relative change <1% (Figure S9b in Supporting Information S1). The effect of vertical mesoscale heat and moisture fluxes on the near-surface moist enthalpy being likely small (Figure 3c), combined with very little change in R_{net} compared to changes in z_i (Figure S10 in Supporting Information S1), lead to the conclusion that BL growth suppression in response to soil moisture heterogeneity is instrumental in amplifying humid heat.

3.4. Dependence to Environmental Conditions

The relationship between soil moisture heterogeneity, boundary layer height, and humid heat involves an array of processes whose relative contributions to changes in the land surface–BL coupling depend on larger-scale environmental conditions. In sensitivity simulations (Table 1 and Text S2 in Supporting Information S1), Twb maxima occur at various locations within the wet patch (Figure S11 in Supporting Information S1). To provide a fair comparison across all sensitivity experiments, wet patch averages of Twb maximum anomalies $\left(\langle \mathrm{Twb}'_{\max} \rangle_\lambda\right)$ are considered hereafter, with the limitation that the *true* Twb maxima may be underestimated. $\langle \mathrm{Twb}'_{\max} \rangle_\lambda$ is

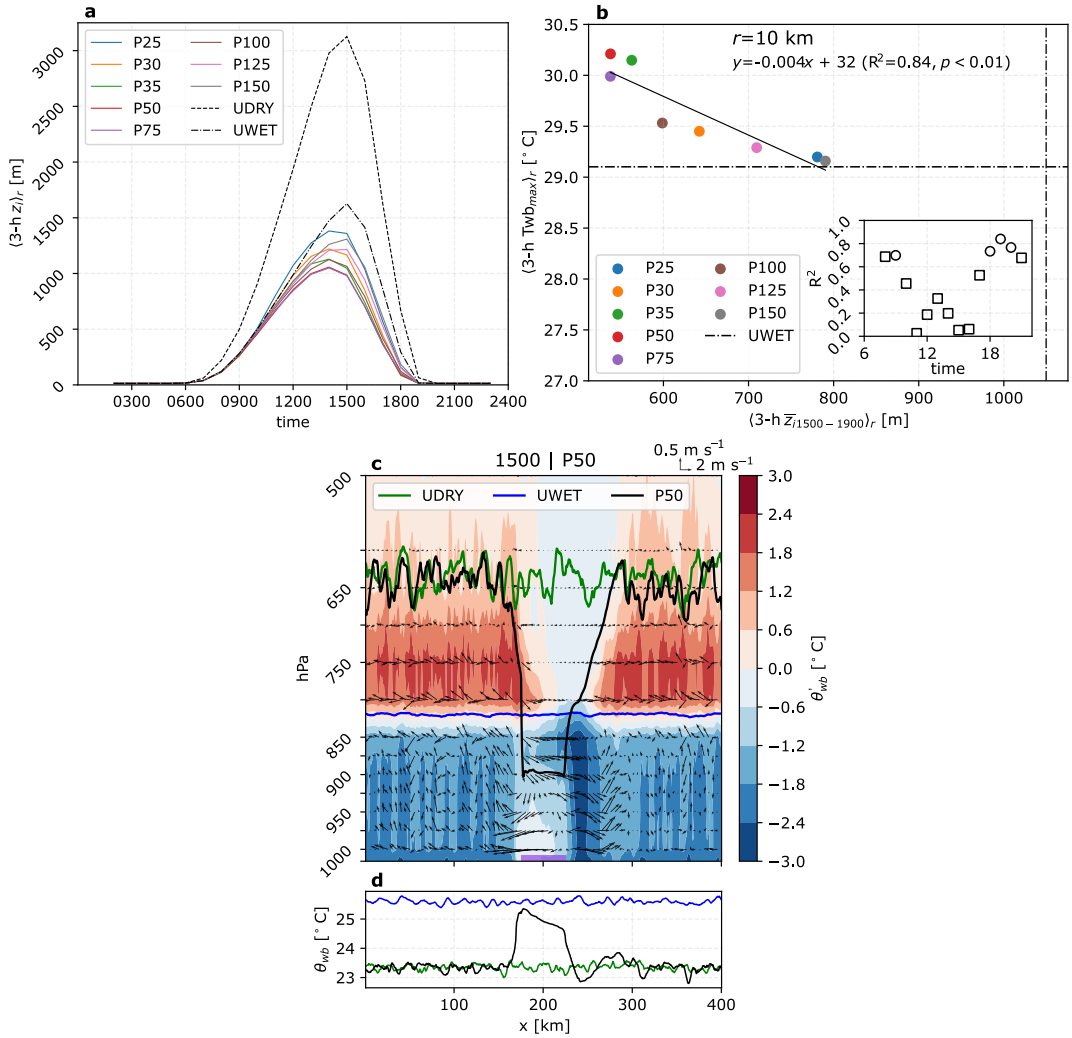

Figure 3. (a) Diurnal cycle of 3-hourly z_i in perturbed experiments (colored lines, see legend), UDRY (dashed line), and UWET (dotted-dashed line). In Pλ, z_i is averaged over the area of maximum Twb (r = 10 km), whereas in UDRY and UWET the domain average is plotted. (b) 3-hourly Twb at 1900 LT as a function of 1500–1900 LT mean 3-hourly BL height in perturbed experiments (dots); both quantities are averaged over a circular area of radius r = 10 km centered on x = x$_0$ + λ/4, as inferred in the previous section. The corresponding domain-mean values in UWET are shown with dotted-dashed lines. The inset in the bottom right corner shows the R^2 of the linear regression between $\langle \mathrm{Twb}_{\max} \rangle_{10}$ sampled at each daytime hour and $\overline{z_i}$ averaged over the 4 preceding hours; significant regressions (at the 1% level) are indicated with circles. (c) Vertical cross section in the longitudinal direction at 1500 LT in P50. Potential wet-bulb temperature anomaly (θ'_{wb}, in °C) is shown with shading and wind anomaly (in m s^{-1}) with arrows (anomalies are calculated as P50-UWET). Solid lines denote z_i in UDRY (green), UWET (blue), and P50 (black). (d) Near-surface θ_{wb} at 1500 LT, with colors similar to the legend in (a). Longitudinal cross section values (panels c and d) are averaged along a 20 km band centered at y$_0$ = 200 km.

calculated as the difference between perturbed and UWET values. $\langle \mathrm{Twb'}_{\max} \rangle_\lambda$ values for the reference setup ("Ref" in Table 1) are also indicated, noting that the maximum value is found for λ = 35 km (Figure 4).

Mesoscale circulations are sensitive to background wind speed, with larger patch sizes required to generate a circulation with higher U, unless the magnitude of the surface heterogeneity (δ) also increases (Segal & Arritt, 1992). The relationship between λ and $\langle \mathrm{Twb'}_{\max} \rangle_\lambda$ is consistent with this theoretical expectation: in $U+$, the critical soil moisture length-scale (λ_c) is shifted toward larger values and the Twb amplification is of similar magnitude as in Ref, but covers a wider range of soil moisture length-scales (Figure 4a). By contrast, in $U-$, λ_c is smaller and $\langle \mathrm{Twb'}_{\max} \rangle_\lambda$ values are reduced. Increased soil moisture contrast ($\delta+$) leads to larger Twb amplification compared to Ref, whereas decreased soil moisture contrast ($\delta-$) results in negative $\langle \mathrm{Twb'}_{\max} \rangle_\lambda$ (Figure 4b).

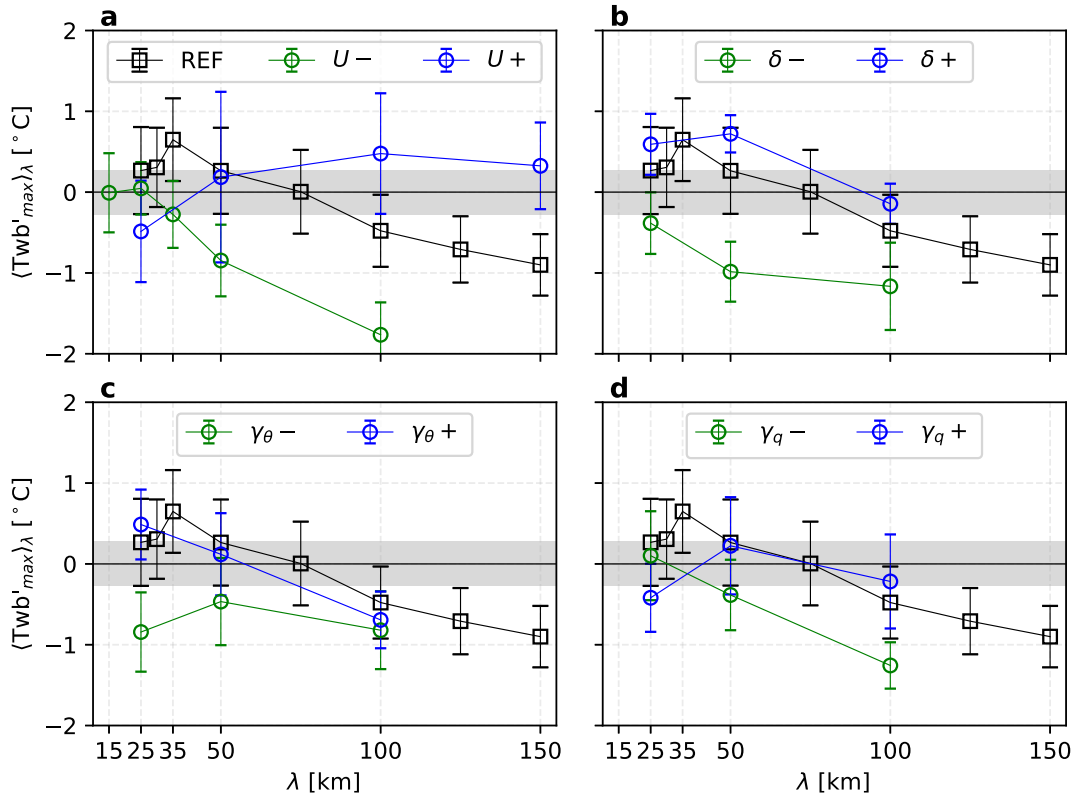

Figure 4. Wet patch averaged maximum Twb anomaly ($\langle Twb'_{max}\rangle_\lambda$, Twb' = $Twb_{P\lambda}$ - Twb_{UWET}; *y*-axis) for different values of soil moisture length-scale (λ; *x*-axis) in various sensitivity experiments (see Table 1): (a) $U-$ and $U+$, (b) $\delta-$ and $\delta+$, (c) $\gamma_\theta-$ and $\gamma_\theta+$, and (d) γ_q- and γ_q+. Within-patch spatial variability is shown with error bars corresponding to $\pm\sigma$ about the spatial mean. Average spatial variability across UWET experiments is shown with gray shading corresponding to $\pm\sigma$ about the zero line.

The sensitivity of BL properties to soil moisture states also depends on the thermodynamical structure of the atmosphere (e.g., Findell & Eltahir, 2003). With decreased atmospheric stability $(\gamma_\theta -)$ the shape of the λ–$\langle Twb'_{max}\rangle_\lambda$ relationship is preserved but $\langle Twb'_{max}\rangle_\lambda$ values are negative (Figure 4c). Increased stability $(\gamma_\theta +)$ yields very similar results to Ref, although no critical λ is found based on the limited number of soil moisture length-scales considered. With increased vertical humidity gradient $(\gamma_q +)$, $\lambda_c \approx 50$ km and $\langle Twb'_{max}\rangle_{\lambda=50}$ is equal to the Ref value (Figure 4d). With reduced vertical humidity gradient $(\gamma_q -)$, $\langle Twb'_{max}\rangle_\lambda$ values decrease with increasing λ and are negative for $\lambda > 25$ km.

Qualitatively similar conclusions can be drawn for HI, a notable exception being the HI amplification in $U-$ for $\lambda \leq 35$ km (Figure S12 in Supporting Information S1). Therefore, the behavior of the relationship between soil moisture length-scale and humid heat in various environments is consistent across a range of humid heat metrics. Other metrics consider the role of wind and radiation in human thermoregulation. In this respect, it should be noted that subsidence can affect both cloud cover and wind speed locally. The net effect of cloud cover reduction—involving changes in longwave and shortwave radiations—on these metrics is difficult to guess, but weaker wind would reduce sweat evaporation rates, enhancing heat stress.

Three additional points should be noted: (a) due to computational limitations, the full range of soil moisture length-scales, for each setup, was not explored, and λ_c in these sensitivity runs may be considered cautiously; (b) the effects of each parameter have been examined separately, and additional simulations are needed to better document the combined effects of U and δ, alongside the thermodynamical structure of the atmosphere, on the land surface–BL coupling and their consequences for humid heat amplification (or lack thereof); (c) the sensitivity to other parameters, such as heterogeneity sharpness and land use, especially to represent urban areas, should be considered in future work.

4. Conclusion

A series of simulations performed with an idealized configuration of a convection-resolving (Δx = 500 m), coupled land-atmosphere model demonstrates that mesoscale soil moisture heterogeneity can amplify humid heat by 1–4°C on scales of 10–20 km across compared to uniform soil moisture. A critical soil moisture length-scale λ_c = 50 km was found, with the background wind speed, the magnitude of the wet–dry contrast, and the vertical profiles of temperature and humidity controlling the relationship between λ_c and humid heat amplification. The most extreme humid heat values are thus more likely over locally wetter soils, as found in Chagnaud et al. (2025) based on a free-running, convective-scale climate model simulation. Numerical weather and climate models that do not represent soil moisture heterogeneity on the key spatial scales of 10–100 km will not simulate the associated mesoscale circulations, nor the humid heat maxima. Such circulations and maxima are also difficult to observe (Bou-Zeid et al., 2020).

Our results point to the possibility of predicting extreme humid heat on city and county scales in regions of strong land-atmosphere coupling, found in the Tropics and beyond (Kong & Huber, 2023; Koster et al., 2004), based on observed soil moisture patterns. Several tropical regions are climatologically close to hazardous physiological thresholds (Matthews, Ramsay, et al., 2025), meaning high quality early warning is essential. This issue is becoming especially pressing as global warming increases temperature and humidity worldwide and shifts environments from energy- to water-limited regimes (Coffel & Lesk, 2024; Denissen et al., 2022; Hsu & Dirmeyer, 2023).

Conflict of Interest

The authors declare no conflicts of interest relevant to this study.

Availability Statement

All simulations were run on ARCHER2, the UK's National Supercomputing Service (Beckett et al., 2024). The simulation outputs are available upon request from the authors on the H2X repository of JASMIN, the UK's collaborative data analysis environment (https://www.jasmin.ac.uk). ERA5 data are available from the Copernicus Climate Change Service (C3S) Climate Data Store (CDS) at Hersbach et al. (2023). The code used to calculate the wet-bulb temperature is available at https://github.com/cr2630git/wetbulb_dj08_spedup. The authors thank the Python community for developing and managing the xarray and matplotlib Python libraries, among many others. The codes used to process the data and plot the figures are available at Chagnaud (2026).

Acknowledgments
The authors thank the two reviewers for their insightful feedback. This work was supported by the NERC (Grant NE/X013618/1 and NE/X013596/1).

References

Barton, E. J., Taylor, C. M., Parker, D. J., Turner, A. G., Belušić, D., Böing, S. J., et al. (2020). A case-study of land–atmosphere coupling during monsoon onset in northern India. *Quarterly Journal of the Royal Meteorological Society*, *146*(731), 2891–2905. https://doi.org/10.1002/qj.3538

Beckett, G., Beech-Brandt, J., Leach, K., Payne, Z., Simpson, A., Smith, L., et al. (2024). *ARCHER2 service description* (Techical Report). Zenodo. https://doi.org/10.5281/zenodo.14507040

Best, M. J., Pryor, M., Clark, D. B., Rooney, G. G., Essery, R. L. H., Ménard, C. B., et al. (2011). The joint UK Land Environment Simulator (JULES), model description – Part 1: Energy and water fluxes. *Geoscientific Model Development*, *4*(3), 677–699. https://doi.org/10.5194/gmd-4-677-2011

Bhumralkar, C. M. (1973). An observational and theoretical Study of atmospheric flow over a heated island: Part I. *Monthly Weather Review*, *101*(10), 719–730. https://doi.org/10.1175/1520-0493(1973)101⟨0719:AOATSO⟩2.3.CO;2

Birch, C. E., Jackson, L. S., Finney, D. L., Marsham, J. M., Stratton, R. A., Tucker, S., et al. (2022). Future changes in African heatwaves and their drivers at the convective scale. *Journal of Climate*, *35*(18), 5981–6006. https://doi.org/10.1175/JCLI-D-21-0790.1

Bou-Zeid, E., Anderson, W., Katul, G. G., & Mahrt, L. (2020). The persistent challenge of surface heterogeneity in boundary-layer meteorology: A review. *Boundary-Layer Meteorology*, *177*(2–3), 227–245. https://doi.org/10.1007/s10546-020-00551-8

Boutle, I. A., Eyre, J. E. J., & Lock, A. P. (2014). Seamless stratocumulus simulation across the turbulent gray zone. *Monthly Weather Review*, *142*(4), 1655–1668. https://doi.org/10.1175/MWR-D-13-00229.1

Bush, M., Flack, D. L. A., Lewis, H. W., Bohnenstengel, S. I., Short, C. J., Franklin, C., et al. (2024). The third met office unified Model-JULES regional atmosphere and land configuration. *RAL3. Copernicus GmbH*. https://doi.org/10.5194/gmd-2024-201

Buzan, J. R., & Huber, M. (2020). Moist heat stress on a hotter Earth. *Annual Review of Earth and Planetary Sciences*, *48*(1), 623–655. https://doi.org/10.1146/annurev-earth-053018-060100

Chagnaud. (2026). guichag/H2X: H2X_v4 [Software]. *Zenodo*. https://doi.org/10.5281/zenodo.19053144

Chagnaud, G., Taylor, C. M., Jackson, L. S., Birch, C. E., Marsham, J. H., & Klein, C. (2025). Wet-bulb temperature extremes locally amplified by wet soils. *Geophysical Research Letters*, *52*(8), e2024GL112467. https://doi.org/10.1029/2024GL112467

Charney, J. G., & Phillips, N. A. (1953). Numerical integration of the quasi-geostrophic equations for barotropic and simple baroclinic flows. *Journal of the Atmospheric Sciences*, *10*(2), 71–99. https://doi.org/10.1175/1520-0469(1953)010⟨0071:NIOTQG⟩2.0.CO;2

Chen, F., & Avissar, R. (1994). The impact of land-surface wetness heterogeneity on mesoscale heat fluxes. *Journal of Applied Meteorology*, *33*(11), 1323–1340. https://doi.org/10.1175/1520-0450(1994)033<1323:tiolsw>2.0.co;2

Chen, L., Achugbu, I. C., Mahmood, R., Kintziger, K., Bell, J. E., & Meredith, G. (2025). Heat stress induced by irrigation over the US Great Plains and related uncertainties. *Environmental Research Letters*, *20*(5), 054072. https://doi.org/10.1088/1748-9326/add029

Coffel, E. D., & Lesk, C. (2024). Recent shift from energy-to moisture-limitation over global croplands. *Environmental Research Letters*, *19*(6), 064065. https://doi.org/10.1088/1748-9326/ad5032

Dalu, G. A., & Pielke, R. A. (1993). Vertical heat fluxes generated by Mesoscale Atmospheric flow induced by thermal inhomogeneities in the PBL. *Journal of the Atmospheric Sciences*, *50*(6), 919–926. https://doi.org/10.1175/1520-0469(1993)050⟨0919:VHFGBM⟩2.0.CO;2

Davies-Jones, R. (2008). An efficient and accurate method for computing the wet-bulb temperature along pseudoadiabats. *Monthly Weather Review*, *136*(7), 2764–2785. https://doi.org/10.1175/2007MWR2224.1

Denissen, J. M. C., Teuling, A. J., Pitman, A. J., Koirala, S., Migliavacca, M., Li, W., et al. (2022). Widespread shift from ecosystem energy to water limitation with climate change. *Nature Climate Change*, *12*(7), 677–684. https://doi.org/10.1038/s41558-022-01403-8

Dharssi, I., Vidale, P. L., Verhoef, A., Macpherson, B., Jones, C., & Best, M. (2009). New soil physical properties implemented in the Unified Model.

Dirmeyer, P. A. (2011). The terrestrial segment of soil moisture-climate coupling. *Geophysical Research Letters*, *38*(16). https://doi.org/10.1029/2011GL048268

Dixon, N. S., Parker, D. J., Taylor, C. M., Garcia-Carreras, L., Harris, P. P., Marsham, J. H., et al. (2013). The effect of background wind on mesoscale circulations above variable soil moisture in the Sahel. *Quarterly Journal of the Royal Meteorological Society*, *139*(673), 1009–1024. https://doi.org/10.1002/qj.2012

Duan, S. Q., Ahmed, F., & Neelin, J. D. (2024). Moist heatwaves intensified by entrainment of dry air that limits deep convection. *Nature Geoscience*, *17*(9), 837–844. https://doi.org/10.1038/s41561-024-01498-y

Edwards, J. M., & Slingo, A. (1996). Studies with a flexible new radiation code. I: Choosing a configuration for a large-scale model. *Quarterly Journal of the Royal Meteorological Society*, *122*(531), 689–719. https://doi.org/10.1002/qj.49712253107

Field, P. R., Hill, A., Shipway, B., Furtado, K., Wilkinson, J., Miltenberger, A., et al. (2023). Implementation of a double moment cloud microphysics scheme in the UK met office regional numerical weather prediction model. *Quarterly Journal of the Royal Meteorological Society*, *149*(752), 703–739. https://doi.org/10.1002/qj.4414

Findell, K. L., & Eltahir, E. A. B. (2003). Atmospheric controls on soil moisture–boundary layer interactions. Part I: Framework development. *Journal of Hydrometeorology*, *4*(3), 552–569. https://doi.org/10.1175/1525-7541(2003)004⟨0552:ACOSML⟩2.0.CO;2

Fletcher, J. K., Birch, C. E., Keane, R. J., Taylor, C. M., & Folwell, S. S. (2022). The effect of Ganges river basin irrigation on pre-monsoon rainfall. *Quarterly Journal of the Royal Meteorological Society*, *148*(747), 3056–3070. https://doi.org/10.1002/qj.4218

Gasparrini, A., Guo, Y., Sera, F., Vicedo-Cabrera, A. M., Huber, V., Tong, S., et al. (2017). Projections of temperature-related excess mortality under climate change scenarios. *The Lancet Planetary Health*, *1*(9), e360–e367. https://doi.org/10.1016/S2542-5196(17)30156-0

Green, J. S. A., & Dalu, G. A. (1980). Mesoscale energy generated in the boundary layer. *Quarterly Journal of the Royal Meteorological Society*, *106*(450), 721–726. https://doi.org/10.1002/qj.49710645005

Gurung, T. R., & Chen, L. (2024). Understanding the influence of soil moisture on heatwave characteristics in the contiguous United States. *Environmental Research Letters*, *19*(6), 064070. https://doi.org/10.1088/1748-9326/ad4dbb

Han, C., Brdar, S., Raasch, S., & Kollet, S. (2019). Large-eddy simulation of catchment-scale circulation. *Quarterly Journal of the Royal Meteorological Society*, *145*(720), 1218–1233. https://doi.org/10.1002/qj.3491

Heerwaarden, C. C. V., & Arellano, J. V. G. D. (2008). Relative humidity as an indicator for cloud formation over heterogeneous land surfaces. *Journal of the Atmospheric Sciences*, *65*(10), 3263–3277. https://doi.org/10.1175/2008JAS2591.1

Hersbach, H., Bell, B., Berrisford, P., Biavati, G., Horányi, A., Muñoz Sabater, J., et al. (2023). ERA5 hourly data on single levels from 1940 to present [Dataset]. https://doi.org/10.24381/cds.adbb2d47

Hersbach, H., Bell, B., Berrisford, P., Hirahara, S., Horányi, A., Muñoz-Sabater, J., et al. (2020). The ERA5 global reanalysis. *Quarterly Journal of the Royal Meteorological Society*, *146*(730), 1999–2049. https://doi.org/10.1002/qj.3803

Hsu, H., & Dirmeyer, P. A. (2023). Soil moisture-evaporation coupling shifts into new gears under increasing CO2. *Nature Communications*, *14*(1), 1162. https://doi.org/10.1038/s41467-023-36794-5

Ivanovich, C. C., Horton, R. M., Sobel, A. H., & Singh, D. (2024). Subseasonal variability of humid heat during the South Asian summer monsoon. *Geophysical Research Letters*, *51*(6), e2023GL107382. https://doi.org/10.1029/2023GL107382

Jackson, L. S., Birch, C. E., Chagnaud, G., Marsham, J. H., & Taylor, C. M. (2025). Daily rainfall variability controls humid heatwaves in the global tropics and subtropics. *Nature Communications*, *16*(1), 3461. https://doi.org/10.1038/s41467-025-58694-6

Kang, S., & Eltahir, E. A. B. (2018). North China Plain threatened by deadly heatwaves due to climate change and irrigation. *Nature Communications*, *9*(1), 2894. https://doi.org/10.1038/s41467-018-05252-y

Kang, S.-L., & Davis, K. J. (2008). The effects of mesoscale surface heterogeneity on the fair-weather convective atmospheric boundary layer. *Journal of the Atmospheric Sciences*, *65*(10), 3197–3213. https://doi.org/10.1175/2008JAS2390.1

Kendon, E. J., Stratton, R. A., Tucker, S., Marsham, J. H., Berthou, S., Rowell, D. P., & Senior, C. A. (2019). Enhanced future changes in wet and dry extremes over Africa at convection-permitting scale. *Nature Communications*, *10*(1), 1794. https://doi.org/10.1038/s41467-019-09776-9

Kong, Q., & Huber, M. (2023). Regimes of soil Moisture–Wet-bulb temperature coupling with relevance to moist heat stress. *Journal of Climate*, *36*(22), 7925–7942. https://doi.org/10.1175/JCLI-D-23-0132.1

Koster, R. D., Dirmeyer, P. A., Guo, Z., Bonan, G., Chan, E., Cox, P., et al. (2004). Regions of strong coupling between soil moisture and precipitation. *Science*, *305*(5687), 1138–1140. https://doi.org/10.1126/science.1100217

Krakauer, N. Y., Cook, B. I., & Puma, M. J. (2020). Effect of irrigation on humid heat extremes. *Environmental Research Letters*, *15*(9), 094010. https://doi.org/10.1088/1748-9326/ab9ecf

Lavender, S. L., Stirling, A. J., Whitall, M., Stratton, R. A., Daleu, C. L., Plant, R. S., et al. (2024). The use of idealised experiments in testing a new convective parametrization: Performance of CoMorph-A. *Quarterly Journal of the Royal Meteorological Society*, *150*(760), 1581–1600. https://doi.org/10.1002/qj.4660

Li, F., & Tamarin-Brodsky, T. (2026). Atmospheric stability sets maximum moist heat and convection in the midlatitudes. *Science Advances*.

Mahrt, L., Sun, J., Vickers, D., Macpherson, J. I., Pederson, J. R., & Desjardins, R. L. (1994). Observations of fluxes and inland breezes over a heterogeneous surface. *Journal of the Atmospheric Sciences*, *51*(17), 2484–2499. https://doi.org/10.1175/1520-0469(1994)051⟨2484:OOFAIB⟩2.0.CO;2

Matthews, T., Ramsay, E. E., Saeed, F., Sherwood, S., Jay, O., Raymond, C., et al. (2025). Humid heat exceeds human tolerance limits and causes mass mortality. *Nature Climate Change*, *15*(1), 4–6. https://doi.org/10.1038/s41558-024-02215-8

Matthews, T., Raymond, C., Foster, J., Baldwin, J. W., Ivanovich, C., Kong, Q., et al. (2025). Mortality impacts of the most extreme heat events. *Nature Reviews Earth & Environment*, *6*(3), 193–210. https://doi.org/10.1038/s43017-024-00635-w

Maybee, B., Klein, C., Taylor, C. M., Burns, H., & Marsham, J. H. (2025). Homogeneous soil moisture fields suppress Sahelian MCS frequency. https://doi.org/10.48550/arXiv.2509.12118

Mishra, V., Ambika, A. K., Asoka, A., Aadhar, S., Buzan, J., Kumar, R., & Huber, M. (2020). Moist heat stress extremes in India enhanced by irrigation. *Nature Geoscience*, *13*(11), 722–728. https://doi.org/10.1038/s41561-020-00650-8

Mitchell, D., Heaviside, C., Vardoulakis, S., Huntingford, C., Masato, G., P Guillod, B., et al. (2016). Attributing human mortality during extreme heat waves to anthropogenic climate change. *Environmental Research Letters*, *11*(7), 074006. https://doi.org/10.1088/1748-9326/11/7/074006

Monteiro, J. M., & Caballero, R. (2019). Characterization of extreme wet-bulb temperature events in Southern Pakistan. *Geophysical Research Letters*, *46*(17–18), 10659–10668. https://doi.org/10.1029/2019GL084711

Ookouchi, Y., Segal, M., Kessler, R. C., & Pielke, R. A. (1984). Evaluation of soil moisture effects on the generation and modification of mesoscale circulations. *Monthly Weather Review*, *112*(11), 2281–2292. https://doi.org/10.1175/1520-0493(1984)112⟨2281:EOSMEO⟩2.0.CO;2

Parker, D. J., Fink, A., Janicot, S., Ngamini, J.-B., Douglas, M., Afiesimama, E., et al. (2008). The Amma Radiosonde Program and its implications for the future of atmospheric monitoring over Africa. *Bulletin of the American Meteorological Society*, *89*(7), 1015–1028. https://doi.org/10.1175/2008BAMS2436.1

Patton, E. G., Sullivan, P. P., & Moeng, C.-H. (2005). The influence of idealized heterogeneity on wet and dry planetary boundary layers coupled to the land surface. *Journal of the Atmospheric Sciences*, *62*(7), 2078–2097. https://doi.org/10.1175/JAS3465.1

Pielke, R. A., Dalu, G. A., Snook, J. S., Lee, T. J., & Kittel, T. G. F. (1991). Nonlinear influence of mesoscale land use on weather and climate. *Journal of Climate*, *4*(11), 1053–1069. https://doi.org/10.1175/1520-0442(1991)004⟨1053:NIOMLU⟩2.0.CO;2

Romps, D. M., & Lu, Y.-C. (2022). Chronically underestimated: A reassessment of US heat waves using the extended heat index. *Environmental Research Letters*, *17*(9), 094017. https://doi.org/10.1088/1748-9326/ac8945

Santanello, J. A., Dirmeyer, P. A., Ferguson, C. R., Findell, K. L., Tawfik, A. B., Berg, A., et al. (2018). Land–Atmosphere interactions: The LoCo perspective. *Bulletin of the American Meteorological Society*, *99*(6), 1253–1272. https://doi.org/10.1175/BAMS-D-17-0001.1

Schwingshackl, C., Hirschi, M., & Seneviratne, S. I. (2017). Quantifying spatiotemporal variations of soil moisture control on surface energy balance and near-surface air temperature. *Journal of Climate*, *30*(18), 7105–7124. https://doi.org/10.1175/JCLI-D-16-0727.1

Segal, M., & Arritt, R. W. (1992). Nonclassical mesoscale circulations caused by surface sensible heat-flux gradients. *Bulletin of the American Meteorological Society*, *73*(10), 1593–1604. https://doi.org/10.1175/1520-0477(1992)073⟨1593:NMCCBS⟩2.0.CO;2

Seneviratne, S. I., Corti, T., Davin, E. L., Hirschi, M., Jaeger, E. B., Lehner, I., et al. (2010). Investigating soil moisture–climate interactions in a changing climate: A review. *Earth-Science Reviews*, *99*(3–4), 125–161. https://doi.org/10.1016/j.earscirev.2010.02.004

Sherwood, S. C. (2018). How important is humidity in heat stress? *Journal of Geophysical Research: Atmospheres*, *123*(21). https://doi.org/10.1029/2018JD028969

Sherwood, S. C., & Huber, M. (2010). An adaptability limit to climate change due to heat stress. *Proceedings of the National Academy of Sciences*, *107*(21), 9552–9555. https://doi.org/10.1073/pnas.0913352107

Steadman, R. G. (1979). The assessment of sultriness. Part I: A temperature-humidity index based on human physiology and clothing science. *Journal of Applied Meteorology and Climatology*, *18*(7), 861–873. https://doi.org/10.1175/1520-0450(1979)018⟨0861:TAOSPI⟩2.0.CO;2

Stratton, R. A., Senior, C. A., Vosper, S. B., Folwell, S. S., Boutle, I. A., Earnshaw, P. D., et al. (2018). A Pan-African convection-permitting regional climate simulation with the met office unified model: CP4-Africa. *Journal of Climate*, *31*(9), 3485–3508. https://doi.org/10.1175/JCLI-D-17-0503.1

Sühring, M., Maronga, B., Herbort, F., & Raasch, S. (2014). On the effect of surface heat-flux heterogeneities on the mixed-layer-top entrainment. *Boundary-Layer Meteorology*, *151*(3), 531–556. https://doi.org/10.1007/s10546-014-9913-7

Taylor, C. M., Parker, D. J., & Harris, P. P. (2007). An observational case study of mesoscale atmospheric circulations induced by soil moisture. *Geophysical Research Letters*, *34*(15), 2007GL030572. https://doi.org/10.1029/2007GL030572

Van Heerwaarden, C. C., Mellado, J. P., & De Lozar, A. (2014). Scaling laws for the heterogeneously heated free convective boundary layer. *Journal of the Atmospheric Sciences*, *71*(11), 3975–4000. https://doi.org/10.1175/JAS-D-13-0383.1

Vanos, J., Guzman-Echavarria, G., Baldwin, J. W., Bongers, C., Ebi, K. L., & Jay, O. (2023). A physiological approach for assessing human survivability and liveability to heat in a changing climate. *Nature Communications*, *14*(1), 7653. https://doi.org/10.1038/s41467-023-43121-5

Vecellio, D. J., Kong, Q., Kenney, W. L., & Huber, M. (2023). Greatly enhanced risk to humans as a consequence of empirically determined lower moist heat stress tolerance. *Proceedings of the National Academy of Sciences*, *120*(42), e2305427120. https://doi.org/10.1073/pnas.2305427120

Vecellio, D. J., Wolf, S. T., Cottle, R. M., & Kenney, W. L. (2022). Evaluating the 35°C wet-bulb temperature adaptability threshold for young, healthy subjects (PSU HEAT Project). *Journal of Applied Physiology*, *132*(2), 340–345. https://doi.org/10.1152/japplphysiol.00738.2021

Vicedo-Cabrera, A. M., Scovronick, N., Sera, F., Royé, D., Schneider, R., Tobias, A., et al. (2021). The burden of heat-related mortality attributable to recent human-induced climate change. *Nature Climate Change*, *11*(6), 492–500. https://doi.org/10.1038/s41558-021-01058-x

Wang, J., Eltahir, E. A. B., & Bras, R. L. (1998). Numerical simulation of nonlinear mesoscale circulations induced by the thermal heterogeneities of land surface. *Journal of the Atmospheric Sciences*, *55*(3), 447–464. https://doi.org/10.1175/1520-0469(1998)055⟨0447:NSONMC⟩2.0.CO;2

Wood, N., Staniforth, A., White, A., Allen, T., Diamantakis, M., Gross, M., et al. (2014). An inherently mass-conserving semi-implicit semi-lagrangian discretization of the deep-atmosphere global non-hydrostatic equations. *Quarterly Journal of the Royal Meteorological Society*, *140*(682), 1505–1520. https://doi.org/10.1002/qj.2235

Yan, D., Li, M., Jiang, X., Lu, Y., Zhou, Y., & Wang, T. (2025). Expanding irrigation intensifies the humid heat stress in China: Evidence from observations and modeling. *Geophysical Research Letters*, *52*(9), e2024GL114241. https://doi.org/10.1029/2024GL114241

Zhang, L., Poll, S., & Kollet, S. (2023). Large-eddy simulation of soil moisture heterogeneity-induced secondary circulation with ambient winds. *Quarterly Journal of the Royal Meteorological Society*, *149*(751), 404–420. https://doi.org/10.1002/qj.4413

Zhang, Y., Held, I., & Fueglistaler, S. (2021). Projections of tropical heat stress constrained by atmospheric dynamics. *Nature Geoscience*, *14*(3), 133–137. https://doi.org/10.1038/s41561-021-00695-3

Zou, L., Shao, D., Zha, Y., Diao, Y., Chen, S., & Gu, W. (2024). Agricultural irrigation exacerbates humid heat stress in the mid-lower reaches of the Yangtze River. *Geophysical Research Letters*, *51*(21), e2024GL110818. https://doi.org/10.1029/2024GL110818